An update on the arrival direction studies made with data from the Pierre Auger Observatory

Geraldina Golup[a,*] **for the Pierre Auger Collaboration**

[a]*CONICET, Centro Atómico Bariloche, Argentina.*

[b]*Observatorio Pierre Auger, Av. San Martín Norte 304, 5613 Malargüe, Argentina*
Full author list: https://www.auger.org/archive/authors_icrc_2023.html

E-mail: spokespersons@auger.org

The search for anisotropies in the arrival directions of ultra-high-energy cosmic rays plays a key role in the efforts to understand their origin. The observed first-harmonic modulation in right ascension above 8 EeV, detected by the Pierre Auger Observatory with a current significance of 6.9σ, suggests an extragalactic origin above this energy. Furthermore, there are indications, at the ~4σ significance level, of anisotropies at intermediate angular scales, which are obtained when comparing the arrival directions against the distribution of potential sources from astrophysical catalogs, in particular that of nearby starburst galaxies, and around the Centaurus region. In this contribution, we present the status of the different searches for anisotropies at small, intermediate and large angular scales. We use the latest available data set, with 19 years of operation that has yielded $135,000$ km^2 yr sr of accumulated exposure, covering the sky at declinations from $-90°$ to $45°$. At small and intermediate scales, we report updates of the all-sky blind search for localized excesses, the study around the Centaurus region, and the likelihood analysis with catalogs of candidate sources. We have also studied the regions of the sky from which the Telescope Array Collaboration has reported hints of excesses in their data and we find no significant effects in the same directions with a data set of comparable size. At large angular scales, the dipolar and quadrupolar amplitudes in energy bins are updated. We discuss the prospects of these searches, both in regards to increases in statistics and in relation to the future inclusion of event-by-event mass estimators in these analyses through the upgrade of the Observatory, AugerPrime.

ICRC2023
38th International Cosmic Ray Conference
The Astroparticle Physics Conference

---

*Speaker

1. Introduction

Thanks to the high-quality data from the Pierre Auger Observatory [1], the world's largest cosmic ray observatory, significant progress has been made in the quest to find the origin of ultra-high-energy cosmic rays (UHECRs). In particular, regarding the arrival direction studies, a dipolar modulation in right ascension (R.A.) at energies above 8 EeV has been established with a significance above 5σ [2]. The direction of this dipole, ~115° away from the Galactic Center, suggests an extragalactic origin of cosmic rays above this energy threshold. Moreover, for lower energies, a change in the equatorial dipole amplitudes and phases has been observed [3]. But, given that the amplitudes are small, these results are not yet statistically significant. However, they are indicative of a transition in the origin of the anisotropies from a galactic one (with phases close to the Galactic Center) to an extragalactic one at energies above a few EeV.

Magnetic deflections are proportional to Z/E, and cosmic rays have a reduced horizon at ultra-high energies. Thus, we also search for small and intermediate-angular-scale anisotropies with the highest-energy events that could help to trace their sources. The Auger Collaboration has reported an excess in the Centaurus region, whose significance has grown steadily since the beginning of the operation of the Observatory [4, 5]. Furthermore, an indication of anisotropy has been reported when searching for correlations with catalogs of potential sources. In particular, the most significant result is for the starburst catalog, which has two galaxies, NGC4945 and M83, in the Centaurus region and one, NGC253, in a region close to the Galactic South Pole, where a mild overdensity has been reported [5, 6]. In this contribution, we present an update of these studies.

2. The data sets

We consider events recorded with the water-Cherenkov surface detectors of the Pierre Auger Observatory. We analyze the events from January 2004 until December 2022. For the transitional years of 2021 and 2022, when the AugerPrime [7] installation was underway, we use only those detectors in which the electronics had not been updated (resulting in the equivalent of 1.6 years of full exposure). For the studies above 32 EeV, we use events with zenith angle $\theta < 80°$, for which we have an exposure of $135,000\,\mathrm{km^2\,yr\,sr}$ and an 85% coverage of the sky. The large-scale analyses above full efficiency of the 1500 m array ($E \geq 4$ EeV) are made considering events with $\theta < 80°$ and with a slightly stricter selection, and removing those that were registered during periods of unreliable data acquisition, resulting in an exposure of $123,000\,\mathrm{km^2\,yr\,sr}$. For the large-scale studies between 0.25 EeV and 4 EeV, we consider only vertical events ($\theta < 60°$, a 71% coverage of the sky) and a stricter quality cut. This data set has an exposure of $81,000\,\mathrm{km^2\,yr\,sr}$. Finally, we also study events with energies down to 0.03 EeV with the 750 m array, with $\theta < 55°$, with an exposure of $337\,\mathrm{km^2\,yr\,sr}$. For more details on the event selection, see e.g. [2, 3, 5]. The events have an angular resolution better than 0.9° for $E > 10$ EeV, and it can degrade up to 1.6° at lower energies [1]. The statistical uncertainty on the energy is ~7% for $E > 10$ EeV and up to ~20% for E ~0.1 EeV, and the systematic uncertainty on the absolute energy scale is 14% [8].

3. Small and intermediate-angular-scale searches

Firstly, we report the results of the blind search for overdensities over the exposed sky. For this, we do a scan in energy in steps of 1 EeV between 32 EeV and 80 EeV and a scan in the top-hat search radius with steps of 1° between 1° and 30°. We compute the binomial probability of measuring the

number of events, N_{obs}, inside a circular window, compared to the mean number of events expected from isotropic simulations, N_{exp}. The post-trial p-value is computed as the fraction of isotropic simulations that have an equal or smaller probability under the same scan. The most significant excess, presented in Table 1, is for an energy threshold of 38 EeV, an angular window of 27°, a post-trial p-value of 2% and for a region located 2° away from Cen A. In Fig. 1, we show the sky maps for local Li-Ma significance and the flux, for the same energy threshold and top-hat window.

Analysis	E_{th} [EeV]	Ψ [°]	N_{obs}	N_{exp}	Local p-value	Post-trial p-value
Overdensity	38	27	245	172.0	1.8×10^{-8}	0.02
Cen A	38	27	237	169.0	1.1×10^{-7}	3.0×10^{-5}

Table 1: Results of the all-sky search for overdensities and the search centered at Cen A. E_{th} is the threshold energy, Ψ is the top-hat radius for which the local p-value is minimum. N_{obs} and N_{exp} are the number of observed and expected events above E_{th} and inside Ψ. The post-trial p-value accounts for the scan.

We also update the search for excesses fixed at the location of Cen A. The energy scan is the same as in the overdensity search and the angular scan as well, with the exception that between 1° and 5°, the steps are of 0.25° as in [4, 5]. The results of the scan are shown in Fig. 2 and the most significant excess is listed in Table 1. The smallest p-value is at the same E_{th} and top-hat window as in [5], and the post-trial p-value has decreased to 3.0×10^{-5} (4.0σ 1-sided). The excess of events has grown by five, within the expectations of a linear growth of the signal, and thus the 5σ discovery threshold is expected for an exposure of $(165,000 \pm 15,000)$ km^2 yr sr, as reported in [5].
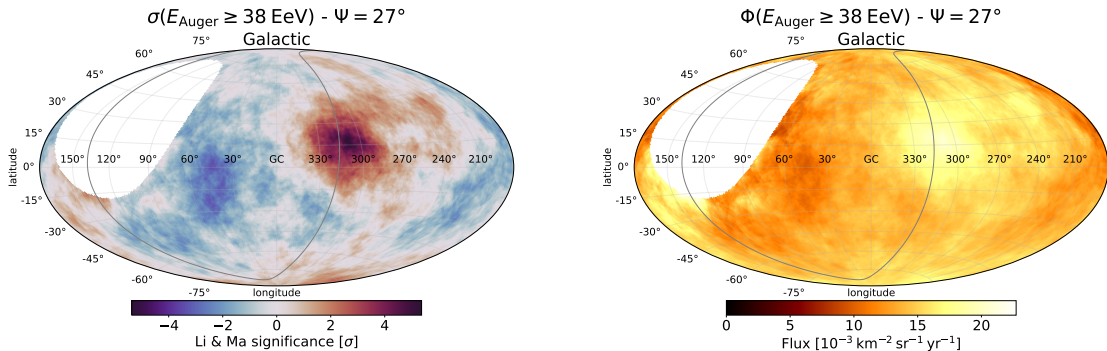

Figure 1: Local Li-Ma significance map within a top-hat window of 27° radius (left panel) and flux map (right panel) with $E \geq 38$ EeV in Galactic coordinates. The supergalactic plane is shown with a gray line.

Furthermore, we study the regions of the sky where the Telescope Array (TA) Collaboration has reported excesses in their data (see [9] for the latest update). The TA overdensities close to the Perseus-Pisces supercluster (PPSC) and the higher-energy excess, the so-called "TA hot spot", are reported for a top-hat window of 20° and 25°, respectively, as in [9]. Their post-trial p-values are between 3.0-3.2σ (for the PPSC results, no account appears to have been taken for the three trials in this region, and the post-trial p-values decrease to ~2.5σ if they search for an excess close to any other major structure). In Table 2, we present our results compared to those published by TA. We have rescaled the energy where TA reports their excesses by -20%, taking into account the cross-calibration of the energy scale reported in [10]. With comparable statistics to TA, we do not find any significant excesses in the same regions with rescaled energy thresholds.
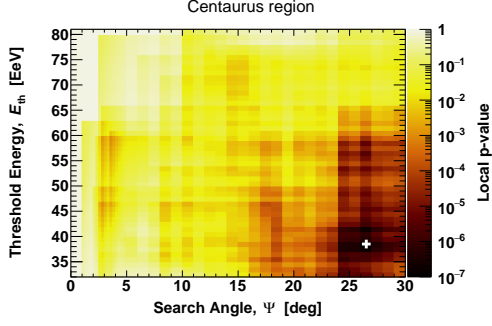
Figure 2: The local p-value for an excess in the Centaurus region as a function of top-hat search angle, Ψ, and energy threshold, E_{th}. The minimum p-value is indicated with a white cross.

	$(\alpha_0, \delta_0)[°]$	E^{TA}	$N_{\text{obs}}^{\text{TA}}$	$N_{\text{exp}}^{\text{TA}}$	$\sigma_{\text{post}}^{\text{TA}}$	E^{Auger}	$N_{\text{obs}}^{\text{Auger}}$	$N_{\text{exp}}^{\text{Auger}}$	$\sigma_{\text{Li-Ma}}^{\text{Auger}}$
PPSC	(17.4, 36.0)	25.1	95	61.4	3.1σ	20.1	68	69.3	-0.2σ
	(19.0, 35.1)	31.6	66	39.1	3.2σ	25.3	40	45.2	-0.8σ
	(19.7, 34.6)	39.8	43	23.2	3.0σ	31.8	27	26.5	0.1σ
TA hot spot	(144.0, 40.5)	57	44	16.9	3.2σ	45.6	7	10.1	-1.0σ

Table 2: Results using Auger data for the regions where TA has reported excesses in their data [9]. (α_0, δ_0) are the equatorial coordinates where TA has observed the overdensity above E^{TA} energy threshold (in EeV). The first three directions correspond to the ones close to the PPSC and the last one corresponds to the so-called "TA hot spot". $N_{\text{obs}}^{\text{TA}}$, $N_{\text{exp}}^{\text{TA}}$ are the observed and expected number of events reported by TA, and $\sigma_{\text{post}}^{\text{TA}}$ is their post-trial significance. $N_{\text{obs}}^{\text{Auger}}$, $N_{\text{exp}}^{\text{Auger}}$, $\sigma_{\text{Li-Ma}}^{\text{Auger}}$ are the corresponding values using Auger data, for the same location and energy threshold $E^{\text{Auger}} = 0.8 \times E^{\text{TA}}$.

Catalog	E_{th} [EeV]	$\Psi[°]$	$\alpha[\%]$	TS	Post-trial p-value
All galaxies (IR)	38	24^{+15}_{-8}	14^{+8}_{-6}	18.5	6.3×10^{-4}
Starbursts (radio)	38	25^{+13}_{-7}	9^{+7}_{-4}	23.4	6.6×10^{-5}
All AGNs (X-rays)	38	25^{+12}_{-7}	7^{+4}_{-3}	20.5	2.5×10^{-4}
Jetted AGNs (γ-rays)	38	23^{+8}_{-7}	6^{+3}_{-3}	19.2	4.6×10^{-4}

Table 3: Most significant results of the catalog-based searches. We show the threshold energy, E_{th}, the equivalent top-hat radius, Ψ, the signal fraction, α, the local test statistic, TS, and the post-trial p-value.

For the catalog-based searches, we apply the same unbinned maximum likelihood method with two free parameters, the Fisher search radius Θ (the equivalent top-hat radius Ψ is $1.59 \times \Theta$) and the signal fraction, α, as in [5, 6]. The energy scan is again in steps of 1 EeV between 32 EeV and 80 EeV. We consider the same four catalogs as in the previous publications and the probability maps are built weighting objects by their relative flux in the corresponding electromagnetic band and an attenuation due to their different distances (following the Auger spectral-composition modeling [11]). The catalogs (and their flux proxies) are: "all galaxies (IR)" from 2MRS (K-band), "starbursts (radio)" based on Lunardini+19 (1.4 GHz), "all AGNs (X-rays)" from Swift-BAT (14-195 keV) and "jetted AGNs (γ-rays)" from Fermi 3FHL ($E > 10$ GeV). The results are shown in Table 3. All excesses happen at the same E_{th} and similar angular window since all models capture the overdensity in the Centaurus region (Cen A or NGC4945 and M83). The starburst model, which also adds

the mild excess in the Galactic South Pole (NGC 253), has the most significant result, with a post-trial p-value that has increased to 6.6×10^{-5} (3.8σ 1-sided) with respect to [5]. This decrease in significance is driven by a decrease in the flux in the region of NGC253, which went from $\Phi_{NGC253} = (12.8 \pm 1.2) \times 10^{-3}\,\text{km}^{-2}\,\text{yr}^{-1}\,\text{sr}^{-1}$ (for $E \geq 40\,\text{EeV}$ and a top-hat window of 25°), in [5], to $\Phi_{NGC253} = (12.2 \pm 1.2) \times 10^{-3}\,\text{km}^{-2}\,\text{yr}^{-1}\,\text{sr}^{-1}$, within its statistical uncertainty. In Fig. 3, we show the test statistic of the starburst model, together with the excess in the Centaurus region, as a function of the exposure of the Observatory. It is seen that the fluctuations for this model are within the 95% C.L. of the expected linear behavior from signal simulations.
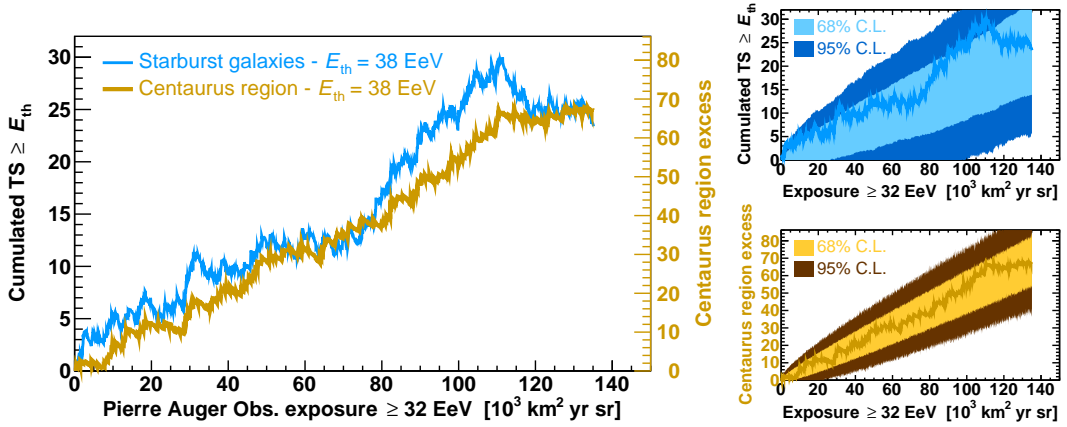
Figure 3: Test statistic of the starburst model and excess in the Centaurus region above the best energy threshold as a function of exposure accumulated by the Pierre Auger Observatory (left panel). The fluctuations around the linear behavior expected from signal simulations are shown in the right panels.

4. Large-angular-scale searches

We present an update of the searches for anisotropies at large angular scales with the current data set. Above full-efficiency of the Observatory, we can perform a combined Fourier analysis in R.A., which is sensitive to the equatorial component of a dipolar anisotropy ($d_\perp$), and in azimuth, which is sensitive to the North-South component (d_z) to make a three-dimensional reconstruction of the dipole. We apply weights that account for the small variations in coverage and the tilt of the array, and the energy of the events has already been corrected for atmospheric and geomagnetic effects for events with zenith angle smaller than 60° (between 60° and 80° the cascades are composed mostly of muons, so the atmospheric effects are less important and the geomagnetic field is already accounted for in their reconstruction). For more details, see e.g. [2]. The results are listed in Table 4, where it is seen that for $E \geq 8\,\text{EeV}$, the significance of the dipolar modulation in R.A. is now at 6.9σ and that the significance of the 8-16 EeV energy bin is 5.7σ. In Fig. 4, we show the flux above 8 EeV and the distribution in R.A. of the normalized rates of events for that energy threshold. Moreover, in Fig. 5, we illustrate the evolution of the dipole direction and amplitude with energy. We perform a fit to the amplitude as a function of energy, $d(E) = d_{10} \times \left(\frac{E}{10\,\text{EeV}}\right)^\beta$, obtaining $d_{10} = 0.049 \pm 0.009$ and $\beta = 0.97 \pm 0.21$ in agreement with previous results [2]. This increase in amplitude is possibly due to particles with higher rigidity being less deflected and nearby non-homogeneously located sources making a larger contribution to the flux (see [2] for references).

In Table 5, we show the results obtained when a quadrupolar component is included to the Fourier combined analysis. We present them for the energy bins where the significance of the dipole

E [EeV]	N	$d_\perp$	d_z	d	α_d [°]	δ_d [°]	$P(\geq d_\perp)$
4-8	118,835	$0.010^{+0.006}_{-0.004}$	-0.014 ± 0.008	$0.017^{+0.008}_{-0.005}$	91 ± 30	-53^{+21}_{-19}	0.15
≥ 8	49,710	$0.058^{+0.009}_{-0.008}$	-0.045 ± 0.012	$0.073^{+0.010}_{-0.008}$	97 ± 8	-37^{+9}_{-9}	7.4×10^{-12}
8-16	36,683	$0.057^{+0.010}_{-0.009}$	-0.030 ± 0.014	$0.065^{+0.012}_{-0.009}$	92 ± 10	-28^{+11}_{-12}	1.2×10^{-8}
16-32	10,288	$0.059^{+0.020}_{-0.015}$	-0.07 ± 0.03	$0.094^{+0.026}_{-0.019}$	93 ± 18	-51^{+13}_{-13}	4.5×10^{-3}
≥ 32	2,739	$0.11^{+0.04}_{-0.03}$	-0.13 ± 0.05	$0.17^{+0.05}_{-0.04}$	143 ± 19	-51^{+14}_{-13}	8.4×10^{-3}

Table 4: Results for the 3D dipole reconstruction above full efficiency. We present, for each energy bin, the number of events, N, the equatorial component of the amplitude, $d_\perp$, the North-South one d_z, the modulus of the amplitude d, the R.A., α_d, and declination, δ_d, of the dipole direction and the probability of getting a larger amplitude from fluctuations of an isotropic distribution $P(\geq d_\perp)$.
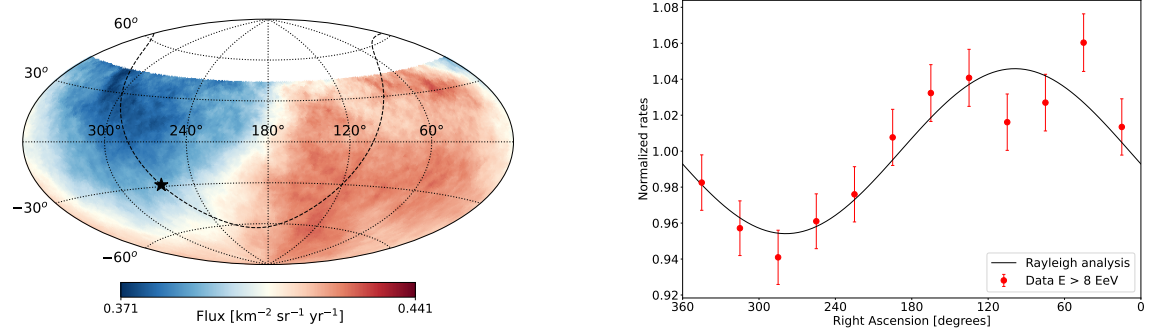
Figure 4: Flux above 8 EeV, smoothed by a top-hat window of $45°$, in equatorial coordinates (left panel). The position of the Galactic Center is shown with a star and the Galactic Plane is indicated with a dashed line. Distribution in R.A. of the normalized rates of events with $E \geq 8$ EeV (right panel). The black line shows the obtained distribution with the Rayleigh analysis assuming only a dipolar component.
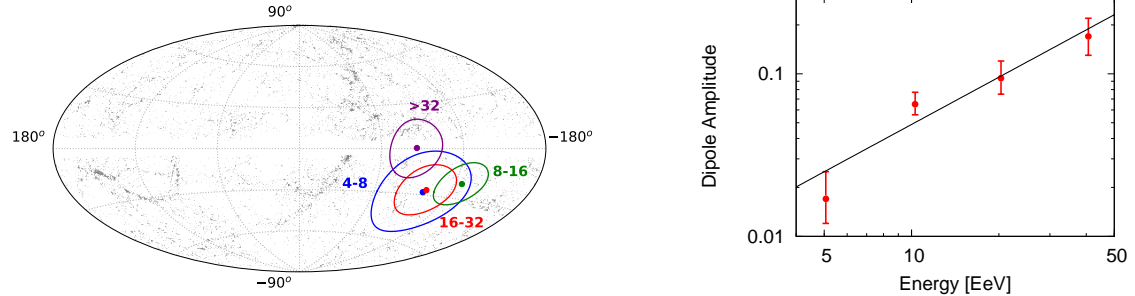

Figure 5: Map with the directions of the 3D dipole for different energy bins, in Galactic coordinates (left panel). We show the contours of equal probability per unit solid angle, marginalized over the dipole amplitude, that contain the 68% CL range. The dots represent the location of the galaxies in the 2MRS catalog within 100 Mpc. The evolution of the dipole amplitude with energy is shown in the right panel.

has surpassed the 5σ discovery level. It is seen that the quadrupolar components are not significant and that the dipolar ones are consistent with the results we obtain assuming only a dipole.

The equatorial component of the dipole can also be reconstructed for lower energies [3]. Below 2 EeV, the East-West method is used for the 1500 m array since trigger effects are difficult to control down to the 1% level. The East-West method, which is based on the difference between the counting rates of the events detected from the east sector and those from the west sector, is less sensitive than

E [EeV]	d_i	Q_{ij}	Q_{ij}
≥ 8	$d_x = -0.002 \pm 0.011$	$Q_{zz} = 0.04 \pm 0.05$	$Q_{xz} = 0.016 \pm 0.025$
	$d_y = 0.059 \pm 0.011$	$Q_{xx} - Q_{yy} = 0.07 \pm 0.04$	$Q_{yz} = 0.005 \pm 0.025$
	$d_z = -0.02 \pm 0.03$	$Q_{xy} = 0.024 \pm 0.019$	
8-16	$d_x = -0.002 \pm 0.012$	$Q_{zz} = 0.10 \pm 0.06$	$Q_{xz} = 0.001 \pm 0.029$
	$d_y = 0.049 \pm 0.012$	$Q_{xx} - Q_{yy} = 0.03 \pm 0.04$	$Q_{yz} = -0.028 \pm 0.029$
	$d_z = 0.02 \pm 0.04$	$Q_{xy} = 0.039 \pm 0.022$	

Table 5: Results for assuming dipolar and quadrupolar components in the two energy bins where the dipole has a significance of over 5σ.

		E [EeV]	N	$d_\perp(\%)$	α_d [°]	P($\geq d_\perp$)	$d_\perp^{UL}(\%)$
SD750	East − West	1/32-1/16	560,474	$1.2^{+0.9}_{-0.5}$	159 ± 40	0.33	3.2
		1/16-1/8	1,230,515	$0.8^{+0.5}_{-0.3}$	-20 ± 33	0.19	2.0
		1/8-1/4	673,514	$0.7^{+0.6}_{-0.3}$	-8 ± 49	0.48	2.0
	Fourier	0.25-0.5	172,171	$0.5^{+0.5}_{-0.2}$	-58 ± 51	0.50	1.6
SD1500	East − West	0.25-0.5	958,899	$0.5^{+0.5}_{-0.2}$	-139 ± 51	0.50	1.6
		0.5 - 1	3,133,596	$0.39^{+0.27}_{-0.16}$	-101 ± 36	0.25	0.99
		1-2	1,683,113	$0.1^{+0.4}_{-0.1}$	-55 ± 99	0.94	0.95
	Fourier	2-4	390,780	$0.7^{+0.3}_{-0.2}$	-17 ± 23	3.7×10^{-2}	1.5

Table 6: Results for the large scale analysis in R.A. We present, for each energy bin, the number of events, N, the equatorial component of the amplitude, $d_\perp$, the R.A. of the dipole direction, α_d, the probability of getting a larger amplitude from fluctuations of an isotropic distribution, P($\geq d_\perp$), and the 99% CL upper limit, $d_\perp^{UL}$.

the Fourier method but the systematics are under better control. For the 0.25-0.5 EeV energy bin, one can also use the data of the 750 m array with the Fourier method and the results are compatible with those of the 1500 m array and the East-West method. For the energy bins below 0.25 EeV, the statistics of the 750 m array are larger than that of the main array, and we apply the East-West method given that for those energies the trigger of the 750 m array is not fully efficient. The results of these analyses are presented in Table 6 and shown in Fig. 6. Even though the results for the lower energies have a probability above 1%, it should be noted that the amplitudes of the equatorial dipole grow from below 1% to above 10% and that the phases shift from close to the Galactic Center to the opposite direction, suggesting a transition of the origin of the anisotropies from galactic to extragalactic.

5. Conclusions and outlook

We have updated the anisotropy searches using arrival directions of UHECRs detected at the Pierre Auger Observatory. For the highest energies, the most significant results are the overdensity at the Centaurus region, with a post-trial p-value of 3.0×10^{-5} (4.0σ) and the likelihood result for the starburst catalog, with a post-trial p-value of 6.6×10^{-5} (3.8σ). With the current growth, the former excess could reach 5σ by the end of 2025 ± 2 years, $(165,000 \pm 15,000)$ km^2 yr sr. The promising inclusion of mass-composition estimators on an event-by-event basis with AugerPrime (and improved mass estimators with Phase 1 data) will give us insight into these excesses.
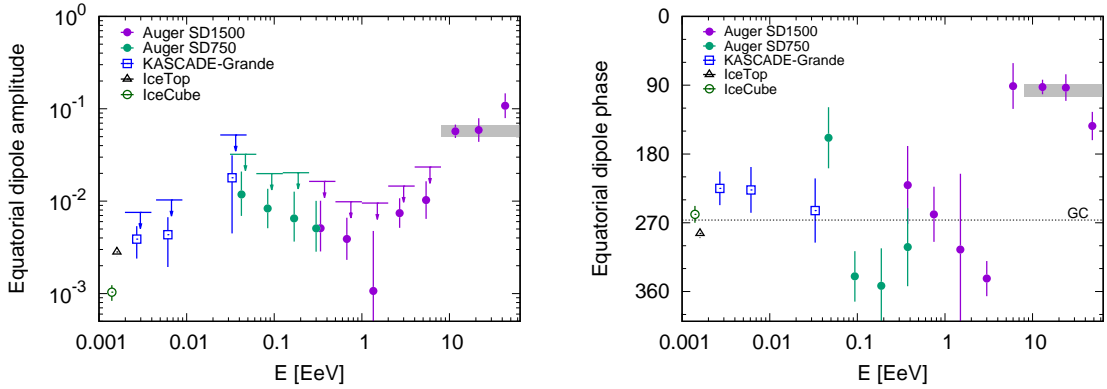
Figure 6: Equatorial dipole amplitude (left panel) and phase (right panel) for the energy bins where we used the 1500 m main surface array (purple circles) and the 750 m infill one (green circles). We show the 99% C.L. upper limits for the energy bins in which the obtained amplitude has a P($\geq d_\perp$)> 1%. Results from IceCube and KASCADE-Grande are also shown for comparison [12].

Furthermore, we have studied the regions in the sky where the TA Collaboration has reported excesses in their data and, with comparable statistics, we have not found any significant results.

Regarding the analyses done for large angular scales, the significance of the equatorial dipole for the ≥ 8 EeV cumulative energy bin is now at 6.9σ and that between 8-16 EeV is now 5.7σ. The quadrupolar moments are not significant. The dipole amplitude increases with energy and with future event-by-event mass-composition estimators, we will be able to study the dipole growth separating the "lighter" and "heavier" events. A difference between the two populations is expected due to their different rigidities. We have computed the equatorial component of the dipole down to 0.03 EeV and the results suggest that the anisotropy has a predominant galactic origin below 1 EeV and a predominant extragalactic one above few EeV. This adds to the indications of an extragalactic origin above 8 EeV when only looking at the direction of the reconstructed 3D dipole at that energy.

References

[1] A. Aab *et al.*, Nucl. Instrum. Meth. A 798 (2015) 172.

[2] A. Aab *et al.*, Science 357 (2017) 1266, Astrophys. J. 868 (2018) 4 and R.M. de Almeida for the Pierre Auger Collaboration, PoS (ICRC2021) 335.

[3] A. Aab *et al.*, Astrophys. J. 891 (2020) 142.

[4] J. Abraham *et al.*, Science 318 (2007) 938, P. Abreu *et al.*, Astropart. Phys. 34 (2010) 314, A. Aab *et al.*, Astrophys. J. 804 (2015) 15.

[5] P. Abreu *et al.*, Astrophys. J. 935 (2022) 170.

[6] A. Aab *et al.*, Astrophys. J. Lett. 853 (2018) L29.

[7] C. Berat for the Pierre Auger Collaboration, EPJ Web Conf. 283 (2023) 06001.

[8] A. Aab *et al.*, Phys. Rev. D 102 (2020) 062005, P. Abreu *et al.*, Eur. Phys. J. C 81 (2021) 966, and A. Aab *et al.*, JINST 15 (2020) P10021.

[9] J. Kim for the Telescope Array Collaboration, EPJ Web of Conferences 283 (2023) 03005.

[10] L. Caccianiga for the Pierre Auger and Telescope Array Collaborations, PoS(ICRC2023)521.

[11] A. Aab *et al.*, JCAP 04 (2017) 009.

[12] R. Abbasi *et al.*, Astrophys. J. 746 (2012) 33, M.G. Aartsen *et al.*, Astrophys. J. 826 (2016) 220, and W.D. Apel *et al.*, Astrophys. J. 870 (2019) 91.

The Pierre Auger Collaboration
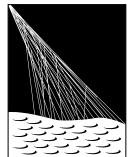
A. Abdul Halim[13], P. Abreu[72], M. Aglietta[54,52], I. Allekotte[1], K. Almeida Cheminant[70], A. Almela[7,12], R. Aloisio[45,46], J. Alvarez-Muñiz[79], J. Ammerman Yebra[79], G.A. Anastasi[54,52], L. Anchordoqui[86], B. Andrada[7], S. Andringa[72], C. Aramo[50], P.R. Araújo Ferreira[42], E. Arnone[63,52], J. C. Arteaga Velázquez[67], H. Asorey[7], P. Assis[72], G. Avila[11], E. Avocone[57,46], A.M. Badescu[75], A. Bakalova[32], A. Balaceanu[73], F. Barbato[45,46], A. Bartz Mocellin[85], J.A. Bellido[13,69], C. Berat[36], M.E. Bertaina[63,52], G. Bhatta[70], M. Bianciotto[63,52], P.L. Biermann[h], V. Binet[5], K. Bismark[39,7], T. Bister[80,81], J. Biteau[37], J. Blazek[32], C. Bleve[36], J. Blümer[41], M. Boháčová[32], D. Boncioli[57,46], C. Bonifazi[8,26], L. Bonneau Arbeletche[21], N. Borodai[70], J. Brack[j], P.G. Brichetto Orchera[7], F.L. Briechle[42], A. Bueno[78], S. Buitink[15], M. Buscemi[47,61], M. Büsken[39,7], A. Bwembya[80,81], K.S. Caballero-Mora[66], S. Cabana-Freire[79], L. Caccianiga[59,49], I. Caracas[38], R. Caruso[58,47], A. Castellina[54,52], F. Catalani[18], G. Cataldi[48], L. Cazon[79], M. Cerda[10], A. Cermenati[45,46], J.A. Chinellato[21], J. Chudoba[32], L. Chytka[33], R.W. Clay[13], A.C. Cobos Cerutti[6], R. Colalillo[60,50], A. Coleman[90], M.R. Coluccia[48], R. Conceição[72], A. Condorelli[37], G. Consolati[49,55], M. Conte[56,48], F. Convenga[41], D. Correia dos Santos[28], P.J. Costa[72], C.E. Covault[84], M. Cristinziani[44], C.S. Cruz Sanchez[3], S. Dasso[4,2], K. Daumiller[41], B.R. Dawson[13], R.M. de Almeida[28], J. de Jesús[7,41], S.J. de Jong[80,81], J.R.T. de Mello Neto[26,27], I. De Mitri[45,46], J. de Oliveira[17], D. de Oliveira Franco[21], F. de Palma[56,48], V. de Souza[19], E. De Vito[56,48], A. Del Popolo[58,47], O. Deligny[34], N. Denner[32], L. Deval[41,7], A. di Matteo[52], M. Dobre[73], C. Dobrigkeit[21], J.C. D'Olivo[68], L.M. Domingues Mendes[72], J.C. dos Anjos, R.C. dos Anjos[25], J. Ebr[32], F. Ellwanger[41], M. Emam[80,81], R. Engel[39,41], I. Epicoco[56,48], M. Erdmann[42], A. Etchegoyen[7,12], C. Evoli[45,46], H. Falcke[80,82,81], J. Farmer[89], G. Farrar[88], A.C. Fauth[21], N. Fazzini[e], F. Feldbusch[40], F. Fenu[41,d], A. Fernandes[72], B. Fick[87], J.M. Figueira[7], A. Filipčič[77,76], T. Fitoussi[41], B. Flaggs[90], T. Fodran[80], T. Fujii[89,f], A. Fuster[7,12], C. Galea[80], C. Galelli[59,49], B. García[6], C. Gaudu[38], H. Gemmeke[40], F. Gesualdi[7,41], A. Gherghel-Lascu[73], P.L. Ghia[34], U. Giaccari[48], M. Giammarchi[49], J. Glombitza[42,g], F. Gobbi[10], F. Gollan[7], G. Golup[1], M. Gómez Berisso[1], P.F. Gómez Vitale[11], J.P. Gongora[11], J.M. González[1], N. González[7], I. Goos[1], D. Góra[70], A. Gorgi[54,52], M. Gottowik[79], T.D. Grubb[13], F. Guarino[60,50], G.P. Guedes[22], E. Guido[44], S. Hahn[39], P. Hamal[32], M.R. Hampel[7], P. Hansen[3], D. Harari[1], V.M. Harvey[13], A. Haungs[41], T. Hebbeker[42], C. Hojvat[e], J.R. Hörandel[80,81], P. Horvath[33], M. Hrabovský[33], T. Huege[41,15], A. Insolia[58,47], P.G. Isar[74], P. Janecek[32], J.A. Johnsen[85], J. Jurysek[32], A. Kääpä[38], K.H. Kampert[38], B. Keilhauer[41], A. Khakurdikar[80], V.V. Kizakke Covilakam[7,41], H.O. Klages[41], M. Kleifges[40], F. Knapp[39], N. Kunka[40], B.L. Lago[16], N. Langner[42], M.A. Leigui de Oliveira[24], Y Lema-Capeans[79], V. Lenok[39], A. Letessier-Selvon[35], I. Lhenry-Yvon[34], D. Lo Presti[58,47], L. Lopes[72], L. Lu[91], Q. Luce[39], J.P. Lundquist[76], A. Machado Payeras[21], M. Majercakova[32], D. Mandat[32], B.C. Manning[13], P. Mantsch[e], S. Marafico[34], F.M. Mariani[59,49], A.G. Mariazzi[3], I.C. Mariş[14], G. Marsella[61,47], D. Martello[56,48], S. Martinelli[41,7], O. Martínez Bravo[64], M.A. Martins[79], M. Mastrodicasa[57,46], H.J. Mathes[41], J. Matthews[a], G. Matthiae[62,51], E. Mayotte[85,38], S. Mayotte[85], P.O. Mazur[e], G. Medina-Tanco[68], J. Meinert[38], D. Melo[7], A. Menshikov[40], C. Merx[41], S. Michal[33], M.I. Micheletti[5], L. Miramonti[59,49], S. Mollerach[1], F. Montanet[36], L. Morejon[38], C. Morello[54,52], A.L. Müller[32], K. Mulrey[80,81], R. Mussa[52], M. Muzio[88], W.M. Namasaka[38], S. Negi[32], L. Nellen[68], K. Nguyen[87], G. Nicora[9], M. Niculescu-Oglinzanu[73], M. Niechciol[44], D. Nitz[87], D. Nosek[31], V. Novotny[31], L. Nožka[33], A Nucita[56,48], L.A. Núñez[30], C. Oliveira[19], M. Palatka[32], J. Pallotta[9], S. Panja[32], G. Parente[79], T. Paulsen[38], J. Pawlowsky[38], M. Pech[32], J. Pękala[70], R. Pelayo[65], L.A.S. Pereira[23], E.E. Pereira Martins[39,7], J. Perez Armand[20], C. Pérez Bertolli[7,41], L. Perrone[56,48], S. Petrera[45,46], C. Petrucci[57,46], T. Pierog[41], M. Pimenta[72], M. Platino[7], B. Pont[80], M. Pothast[81,80], M. Pourmohammad Shahvar[61,47], P. Privitera[89], M. Prouza[32], A. Puyleart[87], S. Querchfeld[38], J. Rautenberg[38], D. Ravignani[7], M. Reininghaus[39], J. Ridky[32], F. Riehn[79], M. Risse[44], V. Rizi[57,46], W. Rodrigues de Carvalho[80], E. Rodriguez[7,41], J. Rodriguez Rojo[11], M.J. Roncoroni[7], S. Rossoni[43], M. Roth[41], E. Roulet[1], A.C. Rovero[4], P. Ruehl[44], A. Saftoiu[73], M. Saharan[80], F. Salamida[57,46], H. Salazar[64], G. Salina[51], J.D. Sanabria Gomez[30], F. Sánchez[7], E.M. Santos[20], E. Santos[32],

F. Sarazin[85], R. Sarmento[72], R. Sato[11], P. Savina[91], C.M. Schäfer[41], V. Scherini[56,48], H. Schieler[41], M. Schimassek[34], M. Schimp[38], F. Schlüter[41], D. Schmidt[39], O. Scholten[15,i], H. Schoorlemmer[80,81], P. Schovánek[32], F.G. Schröder[90,41], J. Schulte[42], T. Schulz[41], S.J. Sciutto[3], M. Scornavacche[7,41], A. Segreto[53,47], S. Sehgal[38], S.U. Shivashankara[76], G. Sigl[43], G. Silli[7], O. Sima[73,b], F. Simon[40], R. Smau[73], R. Šmída[89], P. Sommers[k], J.F. Soriano[86], R. Squartini[10], M. Stadelmaier[32], D. Stanca[73], S. Stanič[76], J. Stasielak[70], P. Stassi[36], S. Strähnz[39], M. Straub[42], M. Suárez-Durán[14], T. Suomijärvi[37], A.D. Supanitsky[7], Z. Svozilikova[32], Z. Szadkowski[71], A. Tapia[29], C. Taricco[63,52], C. Timmermans[81,80], O. Tkachenko[41], P. Tobiska[32], C.J. Todero Peixoto[18], B. Tomé[72], Z. Torrès[36], A. Travaini[10], P. Travnicek[32], C. Trimarelli[57,46], M. Tueros[3], M. Unger[41], L. Vaclavek[33], M. Vacula[33], J.F. Valdés Galicia[68], L. Valore[60,50], E. Varela[64], A. Vásquez-Ramírez[30], D. Veberič[41], C. Ventura[27], I.D. Vergara Quispe[3], V. Verzi[51], J. Vicha[32], J. Vink[83], J. Vlastimil[32], S. Vorobiov[76], C. Watanabe[26], A.A. Watson[c], A. Weindl[41], L. Wiencke[85], H. Wilczyński[70], D. Wittkowski[38], B. Wundheiler[7], B. Yue[38], A. Yushkov[32], O. Zapparrata[14], E. Zas[79], D. Zavrtanik[76,77], M. Zavrtanik[77,76]

——————— • ———————

[1] Centro Atómico Bariloche and Instituto Balseiro (CNEA-UNCuyo-CONICET), San Carlos de Bariloche, Argentina

[2] Departamento de Física and Departamento de Ciencias de la Atmósfera y los Océanos, FCEyN, Universidad de Buenos Aires and CONICET, Buenos Aires, Argentina

[3] IFLP, Universidad Nacional de La Plata and CONICET, La Plata, Argentina

[4] Instituto de Astronomía y Física del Espacio (IAFE, CONICET-UBA), Buenos Aires, Argentina

[5] Instituto de Física de Rosario (IFIR) – CONICET/U.N.R. and Facultad de Ciencias Bioquímicas y Farmacéuticas U.N.R., Rosario, Argentina

[6] Instituto de Tecnologías en Detección y Astropartículas (CNEA, CONICET, UNSAM), and Universidad Tecnológica Nacional – Facultad Regional Mendoza (CONICET/CNEA), Mendoza, Argentina

[7] Instituto de Tecnologías en Detección y Astropartículas (CNEA, CONICET, UNSAM), Buenos Aires, Argentina

[8] International Center of Advanced Studies and Instituto de Ciencias Físicas, ECyT-UNSAM and CONICET, Campus Miguelete – San Martín, Buenos Aires, Argentina

[9] Laboratorio Atmósfera – Departamento de Investigaciones en Láseres y sus Aplicaciones – UNIDEF (CITEDEF-CONICET), Argentina

[10] Observatorio Pierre Auger, Malargüe, Argentina

[11] Observatorio Pierre Auger and Comisión Nacional de Energía Atómica, Malargüe, Argentina

[12] Universidad Tecnológica Nacional – Facultad Regional Buenos Aires, Buenos Aires, Argentina

[13] University of Adelaide, Adelaide, S.A., Australia

[14] Université Libre de Bruxelles (ULB), Brussels, Belgium

[15] Vrije Universiteit Brussels, Brussels, Belgium

[16] Centro Federal de Educação Tecnológica Celso Suckow da Fonseca, Petropolis, Brazil

[17] Instituto Federal de Educação, Ciência e Tecnologia do Rio de Janeiro (IFRJ), Brazil

[18] Universidade de São Paulo, Escola de Engenharia de Lorena, Lorena, SP, Brazil

[19] Universidade de São Paulo, Instituto de Física de São Carlos, São Carlos, SP, Brazil

[20] Universidade de São Paulo, Instituto de Física, São Paulo, SP, Brazil

[21] Universidade Estadual de Campinas, IFGW, Campinas, SP, Brazil

[22] Universidade Estadual de Feira de Santana, Feira de Santana, Brazil

[23] Universidade Federal de Campina Grande, Centro de Ciencias e Tecnologia, Campina Grande, Brazil

[24] Universidade Federal do ABC, Santo André, SP, Brazil

[25] Universidade Federal do Paraná, Setor Palotina, Palotina, Brazil

[26] Universidade Federal do Rio de Janeiro, Instituto de Física, Rio de Janeiro, RJ, Brazil

[27] Universidade Federal do Rio de Janeiro (UFRJ), Observatório do Valongo, Rio de Janeiro, RJ, Brazil

[28] Universidade Federal Fluminense, EEIMVR, Volta Redonda, RJ, Brazil

[29] Universidad de Medellín, Medellín, Colombia

[30] Universidad Industrial de Santander, Bucaramanga, Colombia

[31] Charles University, Faculty of Mathematics and Physics, Institute of Particle and Nuclear Physics, Prague, Czech Republic

[32] Institute of Physics of the Czech Academy of Sciences, Prague, Czech Republic

[33] Palacky University, Olomouc, Czech Republic

[34] CNRS/IN2P3, IJCLab, Université Paris-Saclay, Orsay, France

[35] Laboratoire de Physique Nucléaire et de Hautes Energies (LPNHE), Sorbonne Université, Université de Paris, CNRS-IN2P3, Paris, France

[36] Univ. Grenoble Alpes, CNRS, Grenoble Institute of Engineering Univ. Grenoble Alpes, LPSC-IN2P3, 38000 Grenoble, France

[37] Université Paris-Saclay, CNRS/IN2P3, IJCLab, Orsay, France

[38] Bergische Universität Wuppertal, Department of Physics, Wuppertal, Germany

[39] Karlsruhe Institute of Technology (KIT), Institute for Experimental Particle Physics, Karlsruhe, Germany

[40] Karlsruhe Institute of Technology (KIT), Institut für Prozessdatenverarbeitung und Elektronik, Karlsruhe, Germany

[41] Karlsruhe Institute of Technology (KIT), Institute for Astroparticle Physics, Karlsruhe, Germany

[42] RWTH Aachen University, III. Physikalisches Institut A, Aachen, Germany

[43] Universität Hamburg, II. Institut für Theoretische Physik, Hamburg, Germany

[44] Universität Siegen, Department Physik – Experimentelle Teilchenphysik, Siegen, Germany

[45] Gran Sasso Science Institute, L'Aquila, Italy

[46] INFN Laboratori Nazionali del Gran Sasso, Assergi (L'Aquila), Italy

[47] INFN, Sezione di Catania, Catania, Italy

[48] INFN, Sezione di Lecce, Lecce, Italy

[49] INFN, Sezione di Milano, Milano, Italy

[50] INFN, Sezione di Napoli, Napoli, Italy

[51] INFN, Sezione di Roma "Tor Vergata", Roma, Italy

[52] INFN, Sezione di Torino, Torino, Italy

[53] Istituto di Astrofisica Spaziale e Fisica Cosmica di Palermo (INAF), Palermo, Italy

[54] Osservatorio Astrofisico di Torino (INAF), Torino, Italy

[55] Politecnico di Milano, Dipartimento di Scienze e Tecnologie Aerospaziali , Milano, Italy

[56] Università del Salento, Dipartimento di Matematica e Fisica "E. De Giorgi", Lecce, Italy

[57] Università dell'Aquila, Dipartimento di Scienze Fisiche e Chimiche, L'Aquila, Italy

[58] Università di Catania, Dipartimento di Fisica e Astronomia "Ettore Majorana", Catania, Italy

[59] Università di Milano, Dipartimento di Fisica, Milano, Italy

[60] Università di Napoli "Federico II", Dipartimento di Fisica "Ettore Pancini", Napoli, Italy

[61] Università di Palermo, Dipartimento di Fisica e Chimica "E. Segrè", Palermo, Italy

[62] Università di Roma "Tor Vergata", Dipartimento di Fisica, Roma, Italy

[63] Università Torino, Dipartimento di Fisica, Torino, Italy

[64] Benemérita Universidad Autónoma de Puebla, Puebla, México

[65] Unidad Profesional Interdisciplinaria en Ingeniería y Tecnologías Avanzadas del Instituto Politécnico Nacional (UPIITA-IPN), México, D.F., México

[66] Universidad Autónoma de Chiapas, Tuxtla Gutiérrez, Chiapas, México

[67] Universidad Michoacana de San Nicolás de Hidalgo, Morelia, Michoacán, México

[68] Universidad Nacional Autónoma de México, México, D.F., México

[69] Universidad Nacional de San Agustin de Arequipa, Facultad de Ciencias Naturales y Formales, Arequipa, Peru

[70] Institute of Nuclear Physics PAN, Krakow, Poland

[71] University of Łódź, Faculty of High-Energy Astrophysics, Łódź, Poland

[72] Laboratório de Instrumentação e Física Experimental de Partículas – LIP and Instituto Superior Técnico – IST, Universidade de Lisboa – UL, Lisboa, Portugal

[73] "Horia Hulubei" National Institute for Physics and Nuclear Engineering, Bucharest-Magurele, Romania

[74] Institute of Space Science, Bucharest-Magurele, Romania

[75] University Politehnica of Bucharest, Bucharest, Romania

[76] Center for Astrophysics and Cosmology (CAC), University of Nova Gorica, Nova Gorica, Slovenia

[77] Experimental Particle Physics Department, J. Stefan Institute, Ljubljana, Slovenia

[78] Universidad de Granada and C.A.F.P.E., Granada, Spain

[79] Instituto Galego de Física de Altas Enerxías (IGFAE), Universidade de Santiago de Compostela, Santiago de Compostela, Spain

[80] IMAPP, Radboud University Nijmegen, Nijmegen, The Netherlands

[81] Nationaal Instituut voor Kernfysica en Hoge Energie Fysica (NIKHEF), Science Park, Amsterdam, The Netherlands

[82] Stichting Astronomisch Onderzoek in Nederland (ASTRON), Dwingeloo, The Netherlands

[83] Universiteit van Amsterdam, Faculty of Science, Amsterdam, The Netherlands

[84] Case Western Reserve University, Cleveland, OH, USA

[85] Colorado School of Mines, Golden, CO, USA

[86] Department of Physics and Astronomy, Lehman College, City University of New York, Bronx, NY, USA

[87] Michigan Technological University, Houghton, MI, USA

[88] New York University, New York, NY, USA

[89] University of Chicago, Enrico Fermi Institute, Chicago, IL, USA

[90] University of Delaware, Department of Physics and Astronomy, Bartol Research Institute, Newark, DE, USA

[91] University of Wisconsin-Madison, Department of Physics and WIPAC, Madison, WI, USA

——

[a] Louisiana State University, Baton Rouge, LA, USA

[b] also at University of Bucharest, Physics Department, Bucharest, Romania

[c] School of Physics and Astronomy, University of Leeds, Leeds, United Kingdom

[d] now at Agenzia Spaziale Italiana (ASI). Via del Politecnico 00133, Roma, Italy

[e] Fermi National Accelerator Laboratory, Fermilab, Batavia, IL, USA

[f] now at Graduate School of Science, Osaka Metropolitan University, Osaka, Japan

[g] now at ECAP, Erlangen, Germany

[h] Max-Planck-Institut für Radioastronomie, Bonn, Germany

[i] also at Kapteyn Institute, University of Groningen, Groningen, The Netherlands

[j] Colorado State University, Fort Collins, CO, USA

[k] Pennsylvania State University, University Park, PA, USA

Acknowledgments